resources

MDPI

Article

Low-Quality Coffee Beans Used as a Novel Biomass Source of Cellulose Nanocrystals: Extraction and Application in Sustainable Packaging

Graziela dos Santos Paulino [1,*], Júlia Santos Pereira [2], Clara Suprani Marques [3], Kyssila Vitória Reis Vitalino [1], Victor G. L. Souza [3,4,*], Ananda Pereira Aguilar [1], Lucas Filipe Almeida [1], Taíla Veloso de Oliveira [3,4], Andréa de Oliveira Barros Ribon [1], Sukarno Olavo Ferreira [5], Eveline Teixeira Caixeta Moura [6], Deusanilde de Jesus Silva [7] and Tiago Antônio de Oliveira Mendes [1]

1 Department of Biochemistry and Molecular Biology, Federal University of Viçosa, Av. Peter Henry Rolfs, Viçosa 36570-900, Brazil
2 Department of Biological Sciences, Federal University of Minas Gerais, Av. Presidente Antônio Carlos, Belo Horizonte 31270-901, Brazil
3 Department of Food Science and Tecnology, Federal University of Viçosa, Av. Peter Henry Rolfs, Viçosa 36570-900, Brazil
4 MEtRICs, Departamento de Química, NOVA School of Science and Technology | FCT NOVA, Universidade Nova de Lisboa, Campus de Caparica, 2829-516 Caparica, Portugal
5 Department of Physics, Federal University of Viçosa, Av. Peter Henry Rolfs, Viçosa 36570-900, Brazil
6 Embrapa Café, Parque Estação Biológica, PqEB s/nº, Brasília 70770-901, Brazil
7 Department of Chemistry, Federal University of Viçosa, Av. Peter Henry Rolfs, Viçosa 36570-900, Brazil
* Correspondence: graziela.paulino@ufv.br (G.d.S.P.); v.souza@fct.unl.pt (V.G.L.S.)

Abstract

Most polymeric plastics used as food packaging are obtained from petroleum or made with non-biodegradable synthetic molecules, which slowly degrade and leach into the environment, resulting in the accumulation of microplastics along the trophic chains. To mitigate these impacts, biodegradable packaging derived from agro-industrial biomass residues has emerged as a promising alternative. In this study, bio-based methylcellulose films reinforced with cellulose nanocrystals (CNCs) extracted from low-quality coffee beans were developed and fully characterized. The extracted CNCs presented a needle-like morphology, with an average height of 7.27 nm and a length of 221.34 nm, with 65.75% crystallinity, were stable at pH 7–8, and presented thermogravimetric mass loss of 8.0%. Methylcellulose films containing 0.6% w/w of CNC were produced by casting and characterized in terms of thermal, mechanical, and optical properties. Notably, the incorporation of CNCs resulted in significantly more flexible and less rigid films, as evidenced by the higher elongation at break (57.90%) and lower Young's modulus (0.0015 GPa) compared to neat methylcellulose film. The tensile strength was not affected ($p > 0.05$). Additionally, the MCNC 0.6% films effectively blocked UV light in the 200–300 nm range without compromising transparency. Altogether, these findings underscore the MCNC 0.6% film as a flexible, biodegradable packaging material suitable for food industry application.

Keywords: acid hydrolysis; agro-industrial waste; bioplastics; crystallinity; methylcellulose

check for updates

Academic Editors: Maria Dimopoulou, Athanasios Angelis Dimakis and Antonia Vyrkou

Received: 30 October 2025
Revised: 5 December 2025
Accepted: 11 December 2025
Published: 18 December 2025

Citation: Paulino, G.d.S.; Pereira, J.S.; Marques, C.S.; Vitalino, K.V.R.; Souza, V.G.L.; Aguilar, A.P.; Almeida, L.F.; de Oliveira, T.V.; Ribon, A.d.O.B.; Ferreira, S.O.; et al. Low-Quality Coffee Beans Used as a Novel Biomass Source of Cellulose Nanocrystals: Extraction and Application in Sustainable Packaging. *Resources* **2025**, *14*, 191. https://doi.org/10.3390/resources14120191

Copyright: © 2025 by the authors. Licensee MDPI, Basel, Switzerland. This article is an open access article distributed under the terms and conditions of the Creative Commons Attribution (CC BY) license (https://creativecommons.org/licenses/by/4.0/).

1. Introduction

Cellulose is the most abundant natural polymer found in nature. It is a structural component of the cell wall of plants but is also found in some species of bacteria, such as *Komagataeibacter xylinus*, and even in animals of the phylum Chordata [1,2]. Biochemically, it is

a polymer composed of glucose monomers linked together by β-1,4 glycosidic bond rotated at 180 °C around the central axis, and its basic unit is cellobiose (1-β-D-Glucopyranosyl-4-β-D-glucopyranose). Cellulose type I is the polymorphism found naturally in the cell wall of plants and can be divided into two main allomorphisms: cellulose Iα and Iβ. The Iα allomorphism is mainly found in the primary plant wall of higher plants, while the Iβ allomorphism is found especially inside the secondary plant wall. Both types of cellulose play important roles in the mechanical strength of this structure [2,3].

In addition to serving a structural role in plants, cellulose is widely utilized in technological and biotechnological fields, especially as nanocellulose (NC). Nanocellulose is divided into three main groups: cellulose nanofibers, bacterial nanocellulose, and cellulose nanocrystals [4]. Cellulose nanofiber is composed of flexible cellulose fibrils, which have a crystalline region and an amorphous region in the same fibril. Traditionally, they are manufactured using chemical and/or enzymatic steps, associated with mechanical treatments such as grinding [4,5]. Its physicochemical properties vary depending on the processing method; however, notable characteristics include high flexibility and tenacity, a high aspect ratio, chemical stability, and hydrophilicity. These characteristics make it a good reinforcing agent when associated with hydrophilic polymers [5–7]. Bacterial nanocellulose (BNC) is synthesized by bacteria, especially those of the genus *Gluconacetobacter*, has a high degree of purity, high crystallinity, good elasticity, and is easily biodegraded. Furthermore, BNC can form three-dimensional plots, which allow their application in biomedical devices [7,8].

Finally, cellulose nanocrystals, nanometric, and crystalline particles from the crystalline region of cellulose are mostly produced from vegetable cellulose, using methodologies such as acid hydrolysis and enzymatic hydrolysis, resulting in the digestion of the amorphous part of the cellulose fibrils, preserving only the crystalline region. Therefore, CNCs are highly crystalline, have greater rigidity and elastic modulus, low density, and high aspect ratio [9,10]. Cellulose nanocrystals can be used, for example, as a reinforcing and barrier agent for a variety of plastic films [9,10]. The physical properties of cellulose nanocrystals that contribute the most to such application are their high tensile strength and Young's modulus, which enable them to serve as effective reinforcing agents when combined with other polymers. In the literature, theoretical calculations indicate that the tensile strength of cellulose nanocrystals varies from 2 to 3 GPa, 7.5 to 7.7 GPa, and even 50 to 220 GPa, values similar to those of glasses and metals. These variations are closely related to factors such as degree of crystallinity, geometry, dimensions, and aspect ratio [11,12].

When inserted into a polymeric matrix, the mechanical reinforcement results from the increased number of weak chemical interactions between the cellulose nanocrystals and the polymeric matrix used, such as van der Waals interactions, induced dipole, and ionic interactions. The improvement in mechanical strength increases as the size of the cellulose nanoparticle decreases, since smaller particles are more effective at filling the "empty spaces" between polymer molecules. Cellulose nanocrystals are also known as excellent nanoparticles for chemical modification due to their free -OH groups [13–16].

Currently, the main sources of cellulose nanocrystals are short-fiber cellulosic pulps from wood processing. However, agro-industrial residues, such as corn straw, coffee, barley, rice, fruit husks, and sugar cane, have been explored as potential sources of low-cost cellulose nanocrystals. This approach not only adds value to agricultural production and raw materials but also helps expand markets, generate jobs and income, stimulate innovation and technological development, and support the promotion of the circular economy concept [4].

In this context, Brazil shows great potential for repurposing agricultural waste, as it is among the top five food producers in the world. Moreover, Brazil is the world's largest coffee producer and exporter, accounting for 40% of global production [17]. According to

the Brazilian Ministry of Agriculture, Livestock and Food Supply (MAPA), approximately 55 million 60 kg bags of coffee were processed in Brazil in 2023 [18], with projections for 2032–2033 indicating production around 63 million processed bags, of which 36 million will be exported [19]. The production of this commodity, like other food crops, generates tons of solid and liquid waste. As a common disposal method, solid waste from coffee processing—such as husks, pulp, parchment, and green or spoiled beans—is either burned or left to decompose in open areas. However, both burning and natural degradation of this substantial volume of organic matter lead to the release of greenhouse gases, including CO_2 (carbon dioxide), CH_4 (methane), and N_2O (nitrous oxide). Additionally, they release an excess of nutrients into soil or water bodies, causing an imbalance in the microbiological, plant, and animal biodiversity of the local ecosystem. This promotes processes like the eutrophication of water bodies and the proliferation of vectors and pests that cause animal and/or human diseases, such as mosquitoes [20,21].

To mitigate the negative impacts of improper waste disposal, one of the possibilities is to explore the potential of these wastes for the extraction of cellulose nanocrystals and nanofibers. However, few studies have focused on the extraction of cellulose nanoparticles from coffee residues and their biotechnological application. Some authors, such as Gondim et al. (2024) [22] and Kanai et al. (2020) [23], have demonstrated that cellulose nanocrystals from coffee residues can be used in the production of polymeric film blends. These researchers developed composite films by adding coffee cellulose nanocrystals to polybutylene adipate-co-terephthalate and polyvinyl alcohol polymer matrices, respectively, and obtained potentially promising results.

In this sense, the aim of this work was to expand knowledge about the feasibility of extracting cellulose nanocrystals from discarded coffee beans (low-quality beans) and their applicability as reinforcing agents in biodegradable methylcellulose films. In this study, low-quality coffee beans are defined as those that do not meet the requirements for the production of gourmet and/or specialty coffees. In other words, they fail to meet the physical, sensory, and processing standards demanded for these categories. This includes beans with physical defects—such as broken, black, immature (green), insect-damaged, hollow, or impurity-contaminated beans—as well as poorly processed beans affected by uncontrolled fermentation, irregular drying, mold, or other contaminations that result in undesirable flavors, including sour, earthy, or musty notes. Beans that do not reach the minimum score of 80 points according to the Specialty Coffee Association (SCA) protocol are also considered unsuitable, due to low aromatic complexity, unbalanced acidity, weak body, or excessive bitterness. Finally, lots composed of small, irregular, or highly size-variable beans, falling outside the sieve standards typical of high-quality coffees, are also discarded. Altogether, these factors render such beans inappropriate for gourmet and specialty coffee production, as they compromise uniformity, sensory quality, and the level of excellence expected in these categories.

To this end, cellulose nanocrystals extracted from low-quality coffee beans were characterized regarding their size and morphology (Atomic Force Microscopy (AFM)), aqueous stability (Zeta Potential), functional groups (Fourier transform infrared spectroscopy (FTIR)), crystallinity (X-ray diffraction), and thermal properties (thermogravimetry (TGA)). Subsequently, these nanoparticles were incorporated into the methylcellulose matrix and evaluated for their potential as a reinforcing agent in methylcellulose thin films.

2. Materials and Methods

All reagents used in this work were purchased from Sigma-Aldrich (St. Louis, MO, USA) and include the following: sodium hypochlorite (NaOCl, purity 10–20%), sodium hydroxide (NaOH, purity $\geq$ 97%), hydrogen peroxide (H_2O_2, purity 30–35%), sulfuric

acid (H_2SO_4, purity $\geq$ 95%), methylcellulose (MC, cP 4000, purity 27.5–31.5%), glycerin (purity $\geq$ 99.5%), Tween 80 (purity $\geq$ 98.5%), dimethyl sulfoxide (DMSO, purity $\geq$ 99.5%), and ethanol (purity $\geq$ 95%).

2.1. Plant Biomass Processing

Low-quality Arabica coffee beans (LQCB) were collected from a coffee plantation at Federal University of Viçosa (UFV), in São José do Triunfo, Viçosa, Minas Gerais, Brazil. In the first stage, the beans were washed thrice under running water and immersed for 15 min in sodium hypochlorite solution at 0.5% wt/v. Then, the coffee grains were rewashed under running water until the complete removal of the sanitizing solution. The LQCB were dried in a 45 °C air circulation oven for a period of 48 h, ground in a Model TE-631 knife mill (Tecnal, Piracicaba, Brazil) at 22,500 rpm, and sieved (Ø = 35 mesh). After grinding and sieving, the secondary metabolites were extracted from the coffee beans by the exhaustive percolation method, gradually increasing the polarities of the solvent. The soluble fractions containing secondary metabolites, such as chlorogenic acid, gallic acid, caffeic acid, ferulic acid, 5-caffeoylquinic acid, and vanillic acid, were reserved for further studies on antioxidant and bactericidal activities [24,25]. Subsequently, solid lignocellulosic biomass free of secondary metabolites (CFX) was used to extract cellulose nanocrystals.

2.2. Alkaline Treatment of Plant Biomass

CFX was submitted to alkaline hydrolysis to remove the hemicellulose, lignin, oils, and waxes surrounding plant fibers. In this sense, 50 g of CFX were added to NaOH solution at 4% wt/v and a 1:18 ratio (CFX:NaOH). The mixture was heated to 70 $\pm$ 2 °C under stirring at 145 rpm for 1 h. Next, the plant biomass was filtered using a vacuum filtration system, with the aid of a Büchner Funnel with a 35-mesh aperture. This coffee biomass was washed with distilled water until the washing water reached pH 7.0 and dried at 60 $\pm$ 2 °C for 12 h in a circulatory air oven.

The second stage of the alkaline treatment aimed to remove lignin from plant fibers to purify the pulp content of plant biomass. At this stage, 50 g of previously treated biomass (CFX) were added to H_2O_2/NaOH at 24% v/v and 4% wt/v, respectively, up to a volume of 450 mL. Then, the solution was heated to 50 °C for 2 h under constant stirring at 145 rpm. At the end of the alkaline treatment, the coffee biomass extractive-free and clarified coffee (CFXC) were washed in a filtration funnel vacuum with an opening of 35-mesh, until washing water reached pH 7.0, and were then dried at 60 $\pm$ 2 °C for 12 h in a circulatory air oven.

2.3. Quantification of Lignocellulosic Biomolecules in Fresh and Clarified Coffee Fibers

Cellulose, hemicellulose, lignin, and ash were quantified as described in the "Document number 236/2010 (EMBRAPA)—Procedure for Lignocellulosic Analysis" [26]. The methods recommended in this document are based on a review of the literature and methodologies by TAPPI and ANSI (American National Standards Institute).

2.4. Cellulose Nanocrystal Extraction

The CFXC was crushed in a knife mill (TE-631-Tecnal) until it reached 325 mesh (0.044 mm diameter). Then, 1 g of coffee biomass was added to 13 mL sulfuric acid at 65% wt/v (Sigma Aldrich, St. Louis, MO, USA) at 50 $\pm$ 2 °C for 20 min. The acid hydrolysis reaction was terminated with the addition of 300 mL of refrigerated distilled water at 0 °C. Coffee cellulose nanocrystals (CNCs) were resuspended after 20 cycles of centrifugation at 12,000 rpm at 4 $\pm$ 1 °C. The supernatant containing the CNC was collected, and its pH was adjusted to pH = 5 using NaOH at 0.5 M.

2.5. Atomic Force Microscopy

CNC was suspended in distilled water at a ratio of 1:20 and sonicated for 5 min. Drops of it were placed on mica sheets, followed by drying in an oven at 100 ± 5 °C for 5 min. The mica sheet containing CNC was coupled to the Atomic Force Electron Microscope (AFM) (NT-MDT/Ntegra Prima—Amsterdam, Netherlands) operating in probe scanning mode. The analyses were measured using Nova NT-MDT SPM software system, version 1.0, which allowed the observation of the nanostructures, as well as the determination of their dimensions. The aspect ratio of cellulose nanocrystals was calculated using the following (Equation (1)).

$$AR = \frac{L}{H} \quad (1)$$

where AR corresponds to the aspect ratio, L is the length in nm, and H is the height in nm.

2.6. Fourier Transform Infrared Spectroscopy

The CNC suspensions were dried at 72 ± 2 °C for 24 h, and 1 mg of CNC particles was evaluated for their functional groups in a Fourier transform infrared-attenuated total reflectance (ATR-FTIR) instrument, using the Varian 660-IR equipment coupled to the GLadiATR accessory with a diamond crystal, operating in the sweep transmittance mode in the range of 4000–400 cm^{-1} (Thermo Fisher Scientific, Waltham, MA, USA). Commercial microcrystalline cellulose (MC) was used for comparison purposes under the same conditions as the CNC sample.

2.7. Zeta Potential

Different aliquots of CNC suspensions had their pH adjusted to values from 2 to 12, using 0.5 M NaOH or 0.5 M HCl. The Zeta Potential of CNC suspensions was analyzed at different pH values with the aid of the Zetasizer Malvern Nano ZS (Worcestershire, UK). The analyses were performed at 25 ± 2 °C using a detection angle of 173°, operating at a wavelength of 633 nm.

2.8. X-Ray Diffractometry

X-ray diffractometry (XRD) was performed to determine the crystalline index (CI) of CNC using a BRUKER X-ray diffractometer (D8-Discover, Billerica, MA, USA), with Ni filter and Cu-Kα radiation (λ = 1.5406 Å), angular variation from 10° to 40° (2θ) and 3 min^{-1} speed, 40 kV voltage, and 40 mA current. The crystallinity index (CI) was calculated using the following (Equation (2)):

$$\%CI = \frac{A_t - A_a}{A_t} \times 100 \quad (2)$$

where A_a is the area of the amorphous fraction and A_t is the total area. The identification of the crystalline peaks was calculated using the X Powder X 2021 program [27]. The Full Crystallographic Open Database (COD) was used to identify the type of cellulose present in crystalline structures.

2.9. Thermogravimetry

Thermogravimetry was used to evaluate the thermal decomposition of CNC through the TGA analyzer, model DTG-60 H (Shimadzu, Japan). A sample of 3 mg of nanocrystals was heated in alumina crucibles up to 1000 ± 5 °C, with a heating rate of 10 °C·min^{-1} in an inert nitrogen atmosphere, with a flow rate of 50 mL·min^{-1}.

2.10. Bioplastics Production

Firstly, 1.5 g of methyl cellulose (MC, cP 4000, Sigma Aldrich, St. Louis, MO, USA) was gradually dispersed in 100 mL of a 50% wt/wt solution of ethanol/distilled water at 0 °C

± 2 °C, totaling a 1.5% (wt/wt) dispersion of MC. Subsequently, the mixture was heated at a rate of 5 °C.min^{-1} to a temperature of 70 ± 2 °C under constant stirring at 100 rpm. Once the temperature reached 70 ± 2 °C, 500 µL of glycerin (Sigma Aldrich, St. Louis, MO, USA) and 50 µL of Tween 80 (Sigma Aldrich, St. Louis, MO, USA) were added, corresponding to 33.33% and 3.33% of the polymer mass, respectively. The dispersion was maintained at 70 °C for 15 min under stirring.

The amounts of CNC added to MC dispersions were calculated concerning the polymer mass: 0, 0.6, 1, 3, and 5% (wt/wt). The weighted CNC was dispersed in 5 mL of dimethyl sulfoxide (DMSO) and added to 95 mL of the MC aqueous dispersion (described in the previous paragraph), then cooled in an ice bath until 35 ± 2 °C. The filmogenic dispersions containing cellulose nanocrystals (MCNC) were stirred for 30 min at 100 rpm, and approximately 25 g were poured into 10 cm Petri dishes and dried in an oven for 72 h at 37 ± 2 °C for solvent evaporation.

2.11. Characterization of the Bioplastics

2.11.1. Moisture Content

Before being subjected to moisture content testing, the produced films were stored in vacuum-sealed polyethylene bags and placed in a desiccator containing silica gel as the drying agent. Subsequently, at the time of measuring the moisture content, the bioplastics (Ø = 10 cm) were initially weighed and then placed in an oven at 105 °C for 24 h to attain a constant weight. Next, the dried films were weighed again, and the moisture content was quantified by the difference of the initial and final mass of the films divided by initial mass.

2.11.2. FTIR

A small section of each film was subjected to the attenuated reflectance technique (ATR), using the Varian 660-IR equipment coupled to the GLadiATR accessory with a diamond crystal, operating in transmittance mode, and scanning in the wavelength range of 4000–400 cm^{-1}. All samples (nanocrystal powder and bioplastic films) were dried in a vacuum oven at 90 °C for 24 h and then stored in a desiccator until analysis.

2.11.3. Color Analysis

Bioplastics samples with 25 cm^2 were subjected to color analysis using the L*, a*, b* color coordinates of the CIELAB color scale. The instrument employed was the Colorquest XE Colorimeter (Hunter Lab, Reston, VA, USA) by reflectance, with spherical geometry d/8º, illuminant D65, and observation angle of 10°. Equation (3) below was used for the calculation of the Hue angle (Equation (3)) [28].

$$\text{Hue}^{\text{o}} = 180 + \text{arctang}\left(\frac{\text{b}}{\text{a}}\right) \quad (3)$$

2.11.4. UV-Vis Analysis

Film transparency and UV blocker capability were assessed using a UV-Vis spectrophotometer, model UV 1800 (Shimadzu, Kyoto, Japan). Measurements were taken on 25 cm^2 film samples placed directly in the test cell, with spectral scanning performed over 200–700 nm range. The film's transparency was calculated using Equation (4) [29].

$$\%\,\text{T} = 10^{2-\text{A}} \quad (4)$$

where T = % transparency of the films and A = absorbance in 600 nm of the films.

2.11.5. Scanning Electron Microscopy

Micrographs of the bioplastics surface were obtained using a scanning electron microscope (SEM) with a secondary electron detector operating under low vacuum, model TM 3000 (Hitachi High Technologies America, Inc. Schaumburg, IL, USA). The electron accelerating voltage of 15 Kv and a magnification of 500× were used. Random sections measuring 9 cm^2 from each film were cut and scanned using a scanning electron microscope, with three repetitions of each film.

2.11.6. Thermogravimetry

Termogravimetry (TGA) was used to evaluate the thermal decomposition of the elaborated films. For this purpose, a TGA analyzer was used, model DTG-60 H (Shimadzu, Kyoto, Japan). Samples of 3 mg of bioplastic film were heated in alumina crucibles up to 1000 ± 5 °C at a heating rate of 10 °C·min^{-1} in an inert nitrogen atmosphere and at a flow rate of 50 mL·min^{-1}.

2.11.7. Tensile Test

The thickness of the specimens of the produced films was measured using a digital micrometer (Model 547-401, Mitutoyo, Japan). To determine the thickness, ten random points were chosen from each specimen, and then the average thickness was calculated. The analysis of the mechanical properties of each treatment was conducted with 10 repetitions for each using a Universal Testing Machine (Model 3367, Instron Corporation, Norwood, MA, USA) equipped with a 1 kN load cell. The specimens had rectangular dimensions of 150 mm × 25 mm, with a grip separation distance of 100 mm and a separation rate of 50 mm·min^{-1}, following the standard D882-12 (ASTM, 2012) [30].

2.11.8. Statistical Analysis

Statistical analysis was performed using Origin 2022 SR1 software. The primary tests employed included analysis of variance (ANOVA) for multiple groups' mean comparisons, followed by the Tukey post hoc test for pairwise comparisons. A significance level of 5% ($p < 0.05$) was adopted, and data are presented as mean ± standard error. For each experiment, 10 replicates were used for each sample.

3. Results

3.1. Quantification of Biomolecules

Cellulose, hemicellulose, lignin, ash content, and moisture were quantified in CFX and clarified CFXC, and the results are presented in Table 1.

Table 1. Biomolecule content (%) of coffee biomass: lignocellulosic biomass free of secondary metabolites (CFX) and extractive-free and clarified biomass (CFXC).

Coffee Biomass	Celullose (%)	Hemicellulose (%)	Lignin (%)	Humidity (%)	Ashes (%)
CFX	22.70 ± 0.02	35.80 ± 0.01	36.3 ± 0.4	9.30 ± 0.05	1.00 ± 0.04
CFXC	36.70 ± 0.04	52.70 ± 0.02	17.0 ± 0.0	10.55 ± 0.06	1.80 ± 0.05

It is clear that a 50% reduction in lignin content, a 61.7% increase in cellulose content, and a 147.21% increase in hemicellulose content was obtained in the bleached sample (CFXC). The partial reduction in lignin content and the relative increase in hemicellulose content are explained by the chemical process used to remove lignin and non-cellulosic components. The chosen methodology was alkaline bleaching using H_2O_2/NaOH at concentrations of 24% v/v and 4% wt/v, respectively. Under a relatively high temperature and basic pH conditions, hydrogen peroxide can degrade lignin by hydrolyzing its

phenolic core to carboxylic acid. However, hydrogen peroxide is not efficient in degrading carbohydrates (such as hemicellulose), which are preferably degraded by enzymes. In the presence of alkaline hydrogen peroxide, lignin is degraded, and consequently, there is greater exposure of cellulose and hemicellulose in the plant fibers. The contact of these carbohydrates with alkaline peroxide above 5 vol.% and at moderate temperatures increases their solubility, explaining the increase in hemicellulose content in the CFXC fiber [31,32]. This phenomenon is common in alkaline treatments that remove lignin and amorphous components, thereby increasing the relative concentration of hemicellulose and cellulose in the final material [31]. Thus, this percentage increase is relative to the total weight after the removal of the components and not an absolute increase in hemicellulose. The increase in hemicellulose content after bleaching has been reported in other works, as described by Widjaja et al. (2021) [33], Benali et al. (2024) [34], and Ding et al. (2021) [35].

On the other hand, the 50% reduction in lignin content after the bleaching process is intrinsically related to the process's parameters. The efficiency of bleaching using alkaline peroxide is highly dependent on operational variables, especially concentration, pH, and temperature. These variables interfere with the formation of H_2O_2 radicals, responsible for lignin degradation. Studies such as Melesse et al. (2022) [36] and Rasheed et al. (2024) [37] have demonstrated that additional steps, such as the addition of a diluted acid or base, for example, H_2SO_4 and NaOCl, are necessary to reduce lignin content in plant fibers by 100%, and these methodologies need to be modified according to the nature of the lignocellulosic biomass. After the acid hydrolysis with 65 wt% H_2SO_4, the obtained CNC extraction yield was 21% by mass for each 1 g of hydrolyzed CFXC.

3.2. Fourier Transform Infrared Spectrometry

The FTIR spectra of coffee biomass samples and nanocellulose are depicted in Figures 1A and 1B, respectively.

In Figure 1A, for both samples, the broad band at 3200 cm^{-1} refers to the OH stretching present in cellulose, lignin, and hemicellulose molecules (Table 2). For both CFX and CFXC, the strong peak at 1024 cm^{-1} characterizes the vibration of the C-O-C bond. A relative decrease in its intensity in CFXC compared with CFX indicated that the bleaching process has increased the number of molecules with glycosidic bonds (cellulose and hemicellulose). This observation is supported by the relative increase in cellulose and hemicellulose, which were quantified in the CFXC fibers (Table 1). Still for the samples analyzed in Figure 1A, peaks at 2800 and 2883 cm^{-1} are characteristic of CH_2 stretching. The peaks at 1316 cm^{-1} are attributed to the deformation of the CH bond of the methylene groups, and both chemical groups exhibit cellulose, hemicellulose, and lignin molecules. For the CFXC sample, increased transmission intensity is noted at the wavelengths mentioned above, and decreased transmission intensity is observed at the wavelength of 1024 cm^{-1}, which refers to the vibration of the glycosidic bond. These observations indicate a structural change caused by the oxidation with hydrogen peroxide in an alkaline medium, which possibly led to the demethylation of lignin molecules and, consequently, the relative decrease in lignin; the degradation of lignin increases the exposure of cellulose and hemicellulose in the lignocellulosic fiber, which provides greater solubilization of these components and, consequently, a higher relative content of these carbohydrates in the CFXC fiber [38,39].

For both samples, the absorption at 1234 cm^{-1} is related to the stretching of the C-O bond, and its increased intensity in CFXC may indicate a loss/modification in the phenolic -OH groups. At 1583 cm^{-1}, the region of deformation of the C=C aromatic bond is observed, and the increased intensity indicates the loss of the aromatic structure existing in the lignin molecules. The CFX spectrum has a small and sharp peak at 1713 cm^{-1} that is associated with the ester absorption region, which is abundant in hemicellulose and lignin compounds.

Its absence in the CFXC spectrum corroborates the hypothesis that there was oxidation of lignin [39].

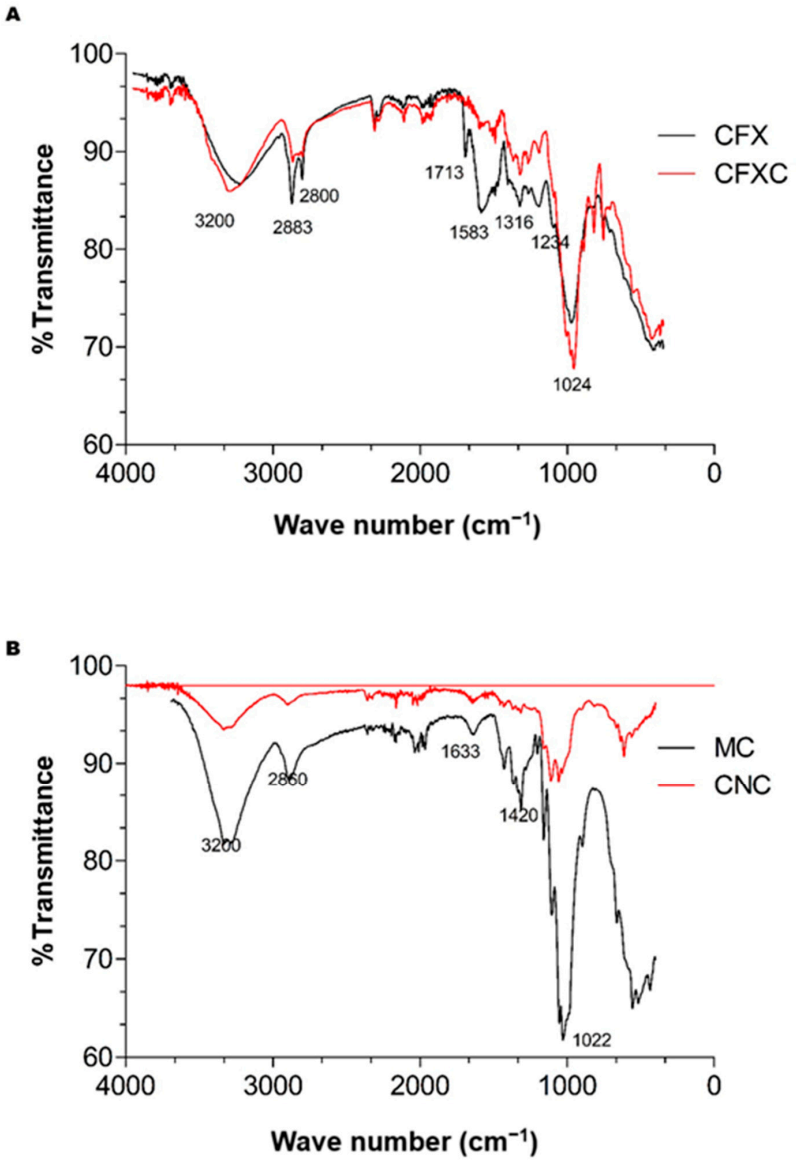

Figure 1. FTIR spectra: (**A**) low-quality coffee beans extractive-free (CFX) and low-quality coffee beans extractive-free and clarified (CFXC). (**B**) cellulose nanocrystals produced from low-quality coffee (CNCs) and commercial microcrystalline cellulose (MC).

In Figure 1B, it is possible to observe two spectra, the extracted CNC and commercial MC, the latter used for comparison purposes. Despite the difference in intensity between the spectra, it is possible to observe that the FTIR profiles match. For both samples, the broad band at 3200 cm^{-1} and the peak at 1633 cm^{-1} refer to the stretching of the OH group. The band centered in the 2860 cm^{-1} region is related to the symmetric and asymmetric stretching of the methyl and methylene groups [40,41]. The peak at 1420 cm^{-1} is attributed to the rocking movement of the C_6 carbon of the glucose monomer [42]. The increased transmission intensity of this peak in the spectrum of the cellulose nanocrystal (CNC) sample, compared to the same peak in the spectrum of the microcrystalline cellulose (MC) sample, indicates the organization of hydrogen bonds in the cellulose structure, which reduces the rocking movement of this group, a typical characteristic of a crystalline structure (cellulose nanocrystals). Finally, the peak at 1022 cm^{-1} of the CNC sample is related to the stretching of the C-O-C group of the hexagonal glucose rings [42–44]. The quantification

of glucose from the cellulose nanocrystals via HPLC supports the cellulose spectrum data obtained by the FTIR. The amount of glucose present in the sample of nanocrystals was 0.212 mg/g (see Supplementary Material S1).

Table 2. Summary of the FTIR analysis.

Wavenumber (cm^{-1})	Vibration/Functional Group	Associated Molecules
3200	OH stretching (broad band)	Cellulose, hemicellulose, lignin
2883 and 2800	CH_2 stretching	Cellulose, hemicellulose, lignin
2860	Symmetric/asymmetric stretching of methyl and methylene groups	Cellulose, hemicellulose, lignin
1713	Carbonyl (C=O) stretching in esters	Hemicellulose, lignin
1633	OH stretching	Cellulose, hemicellulose, water, lignin
1583	Aromatic C=C bending	Lignin aromatic rings
1420	C6 carbon rocking motion in glucose	Cellulose (crystalline structure, CNC)
1316	CH bending	Cellulose, hemicellulose, lignin
1234	C–O stretching	Modification/loss of phenolic-OH in lignin
1024	C–O–C glycosidic bond vibration	Cellulose and hemicellulose
1022	C–O–C stretching of hexagonal glucose rings	Cellulose (CNC, hexose rings)

3.3. Nanoparticle Morphology Characterization

Atomic Force Microscopy (AFM) and Dynamic Light Scattering (DLS) are techniques commonly used to characterize nanoparticles for their dimensions and morphology. In Figure 2, it was possible to observe the dimensions and morphology of the CNC extracted: they were needle-shaped, with an average height of 7.27 nm and an average length of 221.34 nm, which agrees with the values reported in the literature for cellulose nanocrystals. Based on the length, width, and height of the cellulose nanocrystals' values, it is possible to calculate their aspect ratio and obtain information about their surface area, which plays an important role in their applications. Studies on the morphology of CNC proved that the higher the aspect ratio, the better the tensile strength of the compounds reinforced with these nanoparticles, and the greater their chemical reactivity and optical transmittance [45–47]. In this study, the aspect ratio of the CNC was 30.45, which can be considered an average aspect ratio value when compared to those found in the literature.

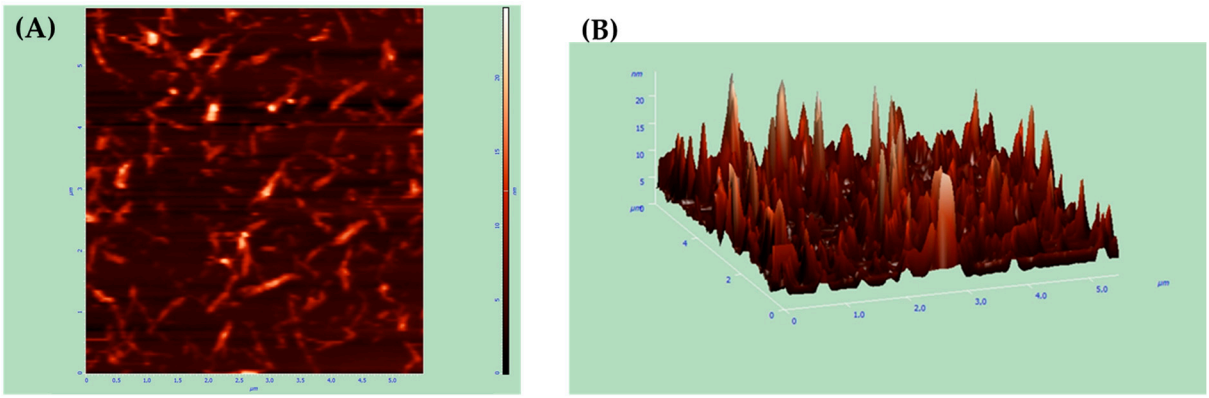

Figure 2. *Cont.*

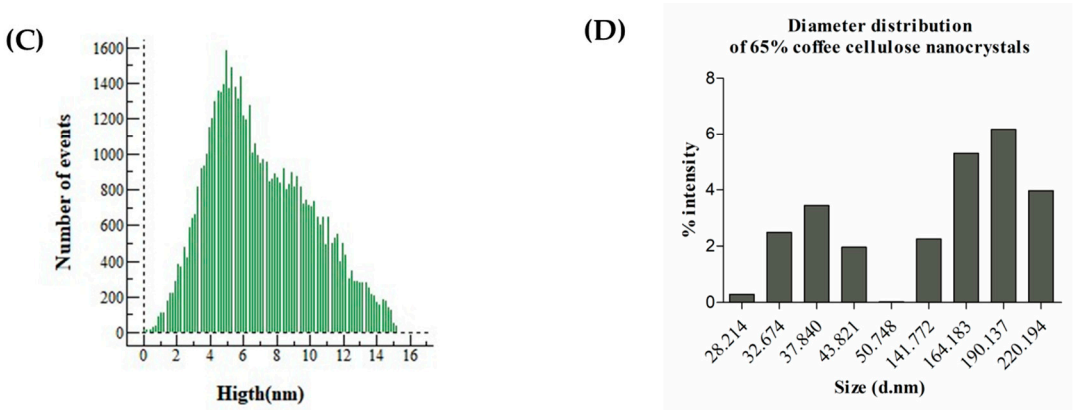

Figure 2. Micrographs from Atomic Force Microscopy (AFM) and data from Dynamic Light Scattering (DLS). (**A**) CNC 1D-AFM, (**B**) CNC 3D-AFM, (**C**) CNC height distribution using AFM, (**D**) CNC width bimodal distribution using DLS.

3.4. Zeta Potential

Stability in aqueous solutions is an important feature of CNC. In general, dispersions with absolute Zeta Potential values greater than 30 mV are more stable with a low tendency to agglomerate, since molecular forces of electrical repulsion are predominant. Suspensions with Zeta Potential values less than 15 mV tend to agglomerate and form clusters. In the present work, coffee CNCs were moderately stable at the pH range between 7 and 8, with Zeta Potential absolute values of 22.5 mV and 20.5 mV, respectively. The values found are consistent with the literature data for the Zeta Potential of CNCs [48,49]. Refer to Supplementary Material S2 for more information on the stability of cellulose nanocrystals extracted from low-quality coffee beans.

3.5. XRD

CNC X-ray diffraction patterns are depicted in Figure 3 and Table 3. The sample presented crystalline peaks at 18–45° and less intense peaks between 45° and 75°. The peaks centered at 2θ 18° and 33.7° are typical of the crystalline portion of cellulose nanocrystals. Another characteristic peak of type IB cellulose nanocrystals is the one centered at 2θ 22°, which, although less intense, is still visible. Peaks in the regions of $50° \leq 2\theta \leq 70°$ are less common in the diffraction pattern of CNCs, probably due to impurities, different shapes and sizes, or the occurrence of more than one type of crystal [50]. Peaks in the region of $50° \leq 2\theta \leq 70°$ are less common in the X-ray diffraction patterns of cellulose nanocrystals. However, studies by Huntley et al. (2015) [51] and Fitriani et al. (2021) [52] presented similar results when characterizing cellulose nanocrystals extracted from wheat straw and pineapple crown, respectively. The peaks in this region may represent type IB cellulose crystallites with different morphologies, such as type IB cellulose crystallites regenerated from type IV cellulose or crystallites with imperfections [51,53]. These peaks may also indicate the presence of type III cellulose, as demonstrated by Huntley et al. (2015) [51], who used the X-ray patterns of type III cellulose available in the SpringerLink database to compare with the X-ray diffraction results of the cellulose nanocrystals produced in their study.

Another hypothesis is the modification of the cellulose structure by the introduction of sulfated ester bonds, which occurs during acid hydrolysis, resulting in the addition of the $-OSO_3H$ group to the cellulose crystals. This changes their structure to "cellulose-OSO_3H" and consequently affects the appearance of the diffractogram. An additional possibility is that these peaks are attributed to the presence of residual Na_2SO_4 crystals, formed after the reaction of residual NaOH from the bleaching step with sulfuric acid (H_2SO_4) from the acid hydrolysis step. Inorganic crystals formed during neutralization, such as Na_2SO_4,

interfere with the diffractogram peaks and may explain those not attributable to cellulose Iβ (peaks at ~2θ that do not correspond to cellulose planes). Anhydrous or hydrated Na_2SO_4 standards frequently exhibit pronounced peaks in ranges compatible with those observed experimentally, making the presence of crystalline salt a plausible explanation for the extra peaks in XRD.

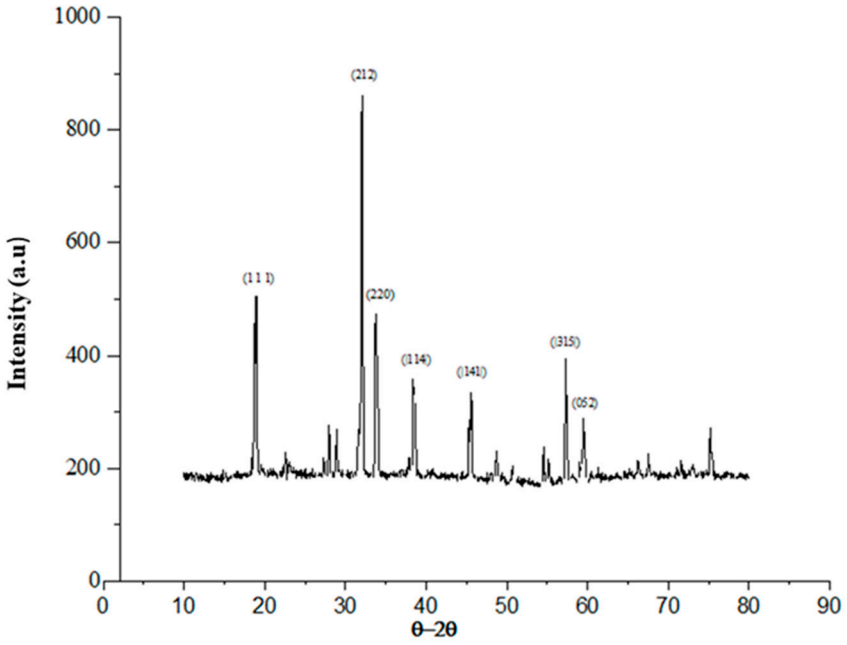

Figure 3. X-ray diffraction pattern of CNCs extracted from discarded coffee beans.

Table 3. Main crystalline peaks of cellulose nanocrystals.

2θ	d-Spacing	2θ	d-Spacing	2θ	d-Spacing
18.9	4.704	32.0	2.795	54.654	1.678
22.57	3.926	33.8	2.649	55.27	1.661
27.29	3.270	38.53	2.339	57.323	1.606
28.0	3.182	45.53	1.988	59.492	1.552
28.9	3.086	48.815			

The crystallinity index was 67.75%, thus corroborating the literature data, with values ranging from 54% to 90%. According to data from the Open Crystallography Database [54], the cellulose nanocrystals extracted in this work are composed of type Iβ cellulose, characteristic of plant biomass, and their crystallite is of the triclinic type. CNC crystallinity is a relevant factor due to its technological application, which affects its physicochemical properties such as tensile strength, rigidity, melting point, permeability to gases and vapors, as well as optical properties. The CNCs extracted in this study presented a medium crystallinity index, which generally allows its use as a reinforcing composite in various biodegradable and synthetic polymer matrices.

3.6. Thermogravimetry

Figure 4 presents the TGA curves of CFXC and CNC samples. The profile of both samples exhibited significant differences in the amount of mass loss and degradation profile. The CFXC sample presents a degradation profile characteristic of cellulosic or lignocellulosic fibers (Figure 4). For this sample, the total degradation was 97.75%, with maximum loss at 315 °C (Figure 4A). The loss of water molecules through dehydration, the evaporation of volatile organic molecules, as well as the degradation of low-molecular-weight organic molecules occurred between 100 and 200 °C, as demonstrated by the presence of the first

degradation peak in Figure 4B. Cellulose degradation in the CFXC sample occurred at 311 °C (Figure 4B), and the physicochemical events involved in this stage are specifically the breaking of hydrogen bonds between parallel cellulose chains and the oxidation of carboxylic groups, which lead to the complete degradation of cellulose into CO_2 and water.

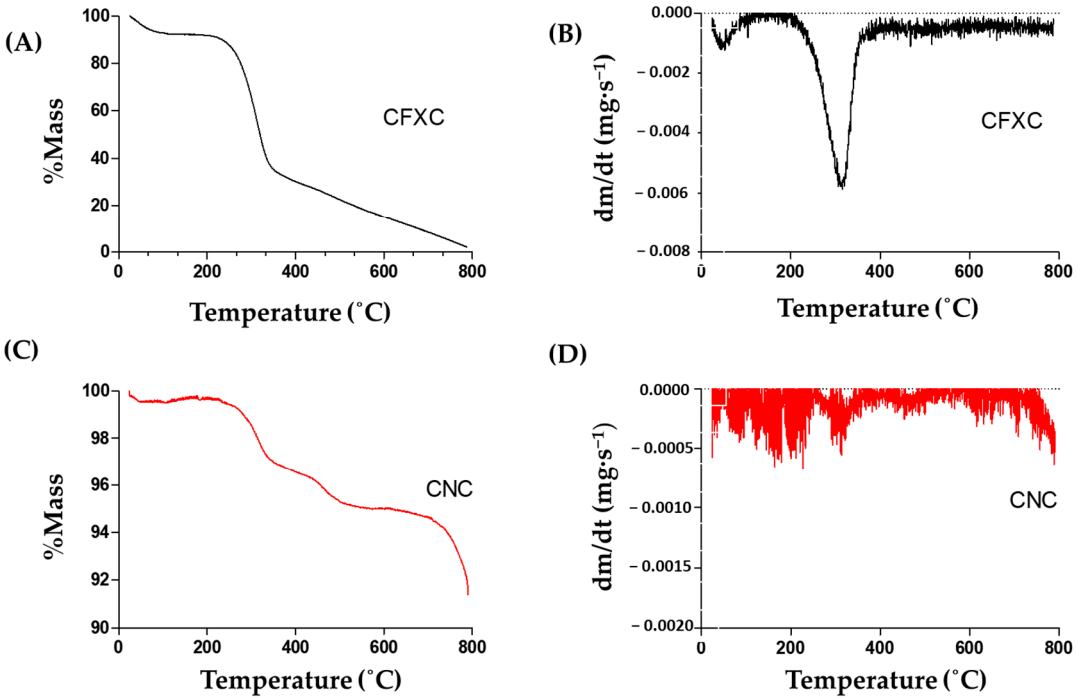

Figure 4. Thermogravimetry. (**A**) TGA of CFXC; (**B**) degradation rate of CFXC; (**C**) TGA of CNC; (**D**) degradation rate of CNC.

CNCs presented higher thermal stability, as the total mass loss during the gradual degradation increased 8% (Figure 4C). The amplification of the thermogravimetric curve revealed two initial events of thermal degradation. The first event occurred between 100 °C and 200 °C and corresponded to the loss of water molecules, evaporation of volatile molecules, and breakdown of low-weight organic molecules (Figure 4D). The second thermal degradation event occurred at 311 °C and corresponded to the degradation of cellulose molecules or lignocellulosic molecules (Figure 4D). Several factors can explain the low mass loss of CNCs, mainly the chemical composition of the biomass, bleaching process, nature of hydrolysis, degree of crystallinity of the nanocrystals, and size of the crystallite [44,49,55,56]. In this work, the main hypothesis to explain the low thermal degradation is the interaction of residual lignin from the bleaching process and the extracted CNCs. Lignin has a slow degradation rate that can vary from 60 to 950 °C, which is justified especially by the complexity of the oxygen groups present in its structure. Each of these functional groups has a degradation temperature, which results in an extensive thermal range for complete lignin degradation. Furthermore, oxygenated groups frequently undergo rearrangements during temperature increases, which generate secondary compounds with high thermal resistance. Another important factor is the presence of inorganic salts, which enhance the natural flame-retardant effect of lignin, thus increasing resistance to thermal degradation [57]. These results corroborate those reported by Farooq (2020) [55], Kanai et al. (2020) [23], and Sabaruddin & Paridah (2018) [58]. In TGA, inorganic salts increase the residual mass, as they do not volatilize within the cellulose degradation range. Therefore, a relatively high residue or a very low total mass loss (e.g., ~8% up to 800 °C) may reflect a significant presence of inorganic content. Furthermore, salts can alter the

shape of the thermal curve, producing plateaus or "tails" at high temperatures and masking organic degradation steps.

3.7. Characterization of Bioplastics

Methylcellulose (MC) control films presented an average moisture content of 10.76%. MC films with added cellulose nanocrystals, on the other hand, exhibited a much lower average moisture content of around 1.40%. Photographs of the produced bioplastics containing different concentrations of CNC are shown in Figure 5. The increased CNC content made the bioplastics more opaque and rigid to the touch. Furthermore, it is possible to observe that the bioplastics containing CNCs were not homogeneous.

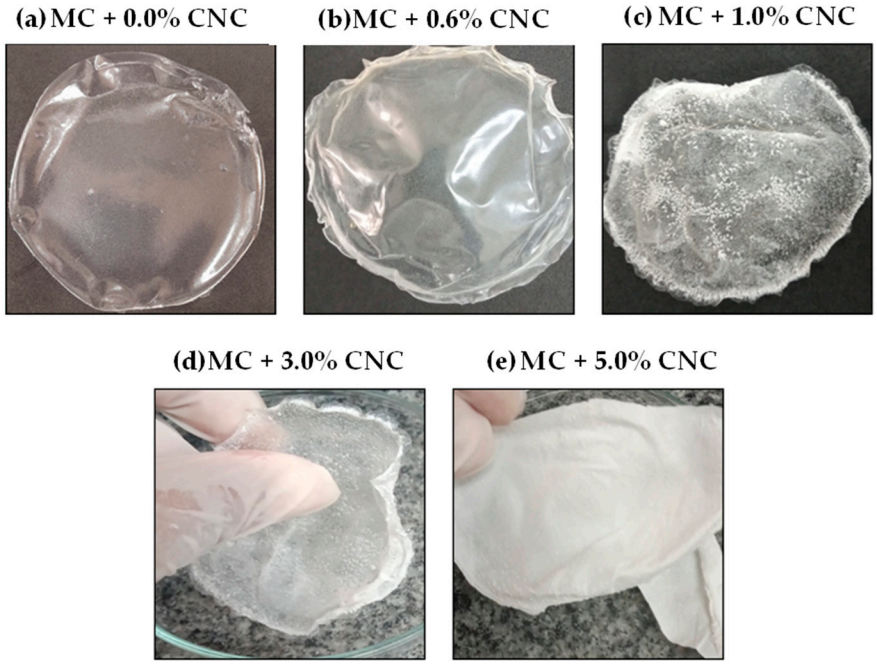

Figure 5. Photographs of methylcellulose (MC) bioplastics incorporated with different concentrations of cellulose nanocrystals produced from low-quality coffee: (**a**) 0% CNC (control); (**b**) 0.6% CNC; (**c**) 1.0% CNC; (**d**) 3.0% CNC; and (**e**) 5.0% CNC. Source: Authors' own work.

In Figure 6, the SEM images show the surface morphology of the produced bioplastics. The control sample (0% of CNC) (Figure 6A) presented a smooth surface with some whitish spots, which were probably lumps of non-gelatinized MC, causing a small irregularity in the produced bioplastic. Shallow tears, which may result from occasional abrasion of bioplastics with hard surfaces during film handling, can also be observed.

Figure 6B–E are the images of those MC bioplastics with increasing concentrations of coffee CNCs. In all micrographs, it is possible to observe CNC agglomerates with different morphologies, in addition to an irregular dispersion of CNCs in the films. In some points, clusters of CNCs with needle-like morphology can be detected, characteristic of the nanoparticle extracted by acid hydrolysis with sulfuric acid. Several factors can cause the agglomeration of cellulose nanocrystals, such as chemical compatibility with the polymeric matrix, shear force, surface energy increase, drying process, temperature or interactions with plasticizers, and other components.

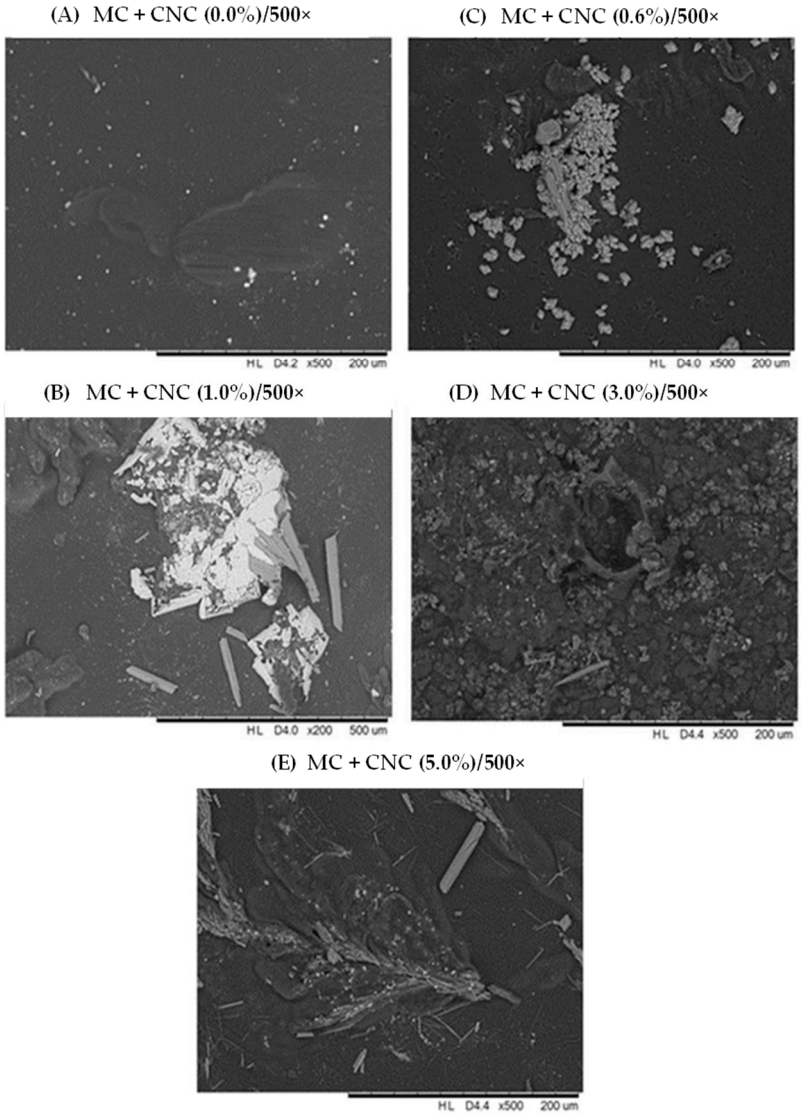

Figure 6. Scanning electron micrographs of methylcellulose bioplastics containing different concentrations cellulose nanocrystals produced from low-quality coffee. (**A**) 0% CNC—magnification 500×; (**B**) 0.6% CNC—magnification 500×; (**C**) 1.0% CNC—magnification 200×; (**D**) 3.0% CNC—magnification 500×; (**E**) 5.0% CNC—magnification 500×.

MC is a cellulose derivative with uncontrolled replacement of the free –OH groups by the $–CH_3$ methyl group. Thus, it is a less-hydrophilic derivative than cellulose. Cellulose nanocrystals, on the other hand, are hydrophilic nanoparticles due to their free –OH groups. Additionally, CNCs extracted with sulfuric acid have negative charges on their surface, derived from the replacement of some free –OH by $–SO_4$ groups, which contributes even more to its hydrophilicity. Therefore, CNC tends to agglomerate and escape from the polymeric matrix and can be physically observed in bioplastics with concentrations of CNCs higher than 0.6%. These films expelled the nanocrystals from the polymeric matrix, causing the dry bioplastic to contain a thin layer of whitish and shiny powder on its surface, which can possibly be the cellulose nanocrystals added to the filmogenic dispersion.

When cellulose nanocrystals are agglomerated, they can acquire different morphologies, as observed by several authors [52,59–61]. The most common morphologies found in groups of CNCs are spherical, cylindrical, and sheet-shaped. The films produced here present spherical agglomeration and cylindrical CNCs.

The FTIR spectra of MC and MCNC exhibited a typical cellulose spectrum (Figure 7). For both samples, the peak at 2950 cm^{-1} is the result of symmetric and asymmetric stretching of the C–H bond. Peaks around 1350–1650 cm^{-1} are related to the deformation in the plane of the δ(C–H) bond, whereas the peak at 1068 cm^{-1} is typical of the stretching of the C–O–C glycosidic bond. The broad band at 3400 cm^{-1} is the result of the stretching vibration of the ν(O-H) bond. The peak that identifies methylcellulose is 950 cm^{-1}, corresponding to the $–OCH_3$ radical of methyl cellulose.

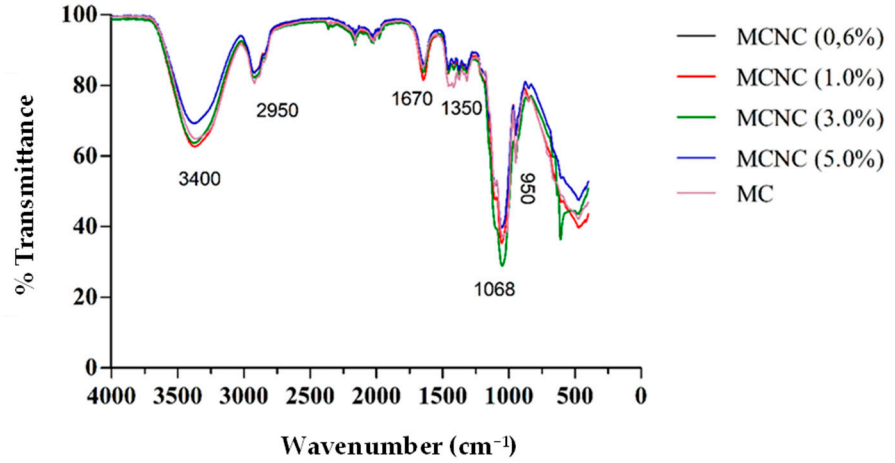

Figure 7. FTIR spectra of the produced methylcellulose (MC) bioplastics and films containing different concentrations of cellulose nanocrystals produced from low-quality coffee (MCNC). Note: The percentages indicate the mass amount of cellulose nanocrystals (CNCs) added to the methylcellulose films.

After evaluation by SEM and FTIR, the chosen concentration of CNC for application in MC bioplastics was 0.6% (wt/wt), due to the homogeneous distribution of cellulose nanoparticles and good malleability during touch. Therefore, the following characterizations refer to MCNC 0.6% films.

3.7.1. Color and UV Blocker Analyses

MC and MCNC bioplastics did not differ significantly ($p > 0.05$) for luminosity index (L) (around 66.7). Regarding the CIELab coordinates a* and b*, produced bioplastics presented as greenish yellow, with the color coordinates for the MCNC 0.6% a* = −1.79, b* = 5.39, and HUE° = 108.87°; for pure MC films, the color coordinates were a*= −2.46, b*= 6.42, and HUE° = 110.97°. The UV blocker analysis (Figure 8A) demonstrated that MCNC 0.6% bioplastics had a UV protection range between 225 and 375 nm greater than MC bioplastics. Proportionally similar results can be seen for the UV/Vis absorption of films containing different concentrations of cellulose nanocrystals from low-quality coffee beans. It is observed that increasing the concentration of cellulose nanocrystals causes an increase in UV light blocking. The highest concentration of cellulose nanocrystals (MCNC film 5%) completely blocks the passage of UV light and drastically reduces the transparency of the film. The UV light blocking capacity of films containing cellulose nanocrystals can be explained by the size distribution of the cellulose nanoparticles produced, which have nanometric dimensions close to or equal to the wavelength of the ultraviolet spectrum. Therefore, it is capable of absorbing certain wavelengths of UV radiation [62]. Furthermore, the cellulose nanocrystals produced in this work are not completely free of lignin (Table 1). The lignin molecules have a phenolic structure, capable of absorbing UV radiation [63,64]; therefore, the increase in the concentration of cellulose nanocrystals also results in an

increase in the concentration of lignin in the film, providing greater UV protection as the concentration of cellulose nanocrystals increases.

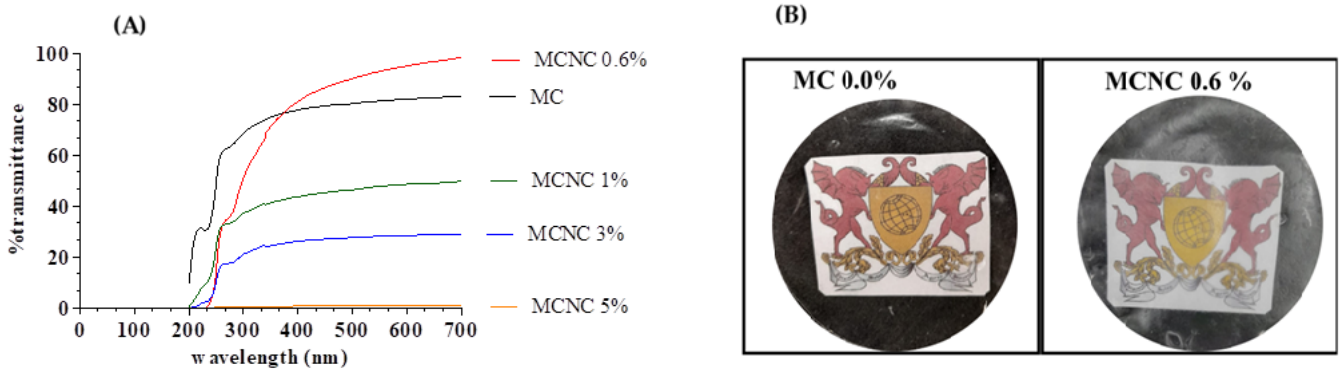

Figure 8. (**A**) Comparison of transmittance UV-Vis percentages of films with increasing percentages of CNC. The samples are MC 0% (line black); MCNC 0.6% (line red); MCNC 1% (line green); MCNC 3% (line blue); and MCNC 5% (line orange). (**B**) Photograph comparing the transparency of the control film (MC 0.0%) and the film containing CNC (MCNC 0.6%). Note: The percentages indicate the percentage of cellulose nanocrystals (CNC) added to the methylcellulose films. Source: Authors' own work.

Transparency of the produced films with or without CNCs is observed in Figure 8B. When analyzing the results of the transparency test at 600 nm and applying the T-test with $p < 0.05$, it is observed that the film containing cellulose nanocrystals exhibits higher transparency than the pristine methylcellulose film. The transparency percentage is 82.04 ± 0.010 for the control and 95.07 ± 0.19 for the film containing cellulose nanocrystals (MCNC 0.6%). Despite visually appearing more opaque, the film with cellulose nanocrystals at 0.6% exhibits higher transmittance than the control film (MC 0.0%). The UV-blocking analysis (Figure 8A) showed that the 0.6% MCNC bioplastics exhibit greater protection in the 225–375 nm range when compared exclusively to MC bioplastics (without nanocrystals). This increased UV protection is primarily attributed to the presence of residual lignin conjugated to the cellulose nanocrystals. As shown in Table 1, the nanocrystals produced in this study retain a fraction of lignin, whose phenolic structure is capable of absorbing UV radiation. Thus, the higher the concentration of cellulose nanocrystals incorporated into the film, the higher the lignin content and, consequently, the greater the UV protection [63,64].

On the other hand, when comparing different nanocrystal concentrations within the MCNC films themselves, it is evident that higher concentrations (such as in the 5% MCNC film) enhance UV blocking but also reduce transparency. In contrast, the 0.6% MCNC film maintains superior transparency not only relative to the 5% MCNC film but also when compared to pure methylcellulose (MC) films, as shown in Figure 8B. This increased transparency occurs because the cellulose nanocrystals exhibit a size distribution smaller than the wavelength of visible light, which minimizes light absorption and allows higher transmittance. Additionally, the UV/Vis spectrophotometer does not distinguish scattered light from directly transmitted light, recording both as total transmittance. Previous studies, such as those by Kim et al. (2015) [65] and Leppänen et al. (2022) [62], reported similar effects in plastic films enhanced with cellulose nanocrystals.

3.7.2. Thermogravimetric

No significant difference in the degradation temperature between MC (Tonset = 179 °C Tmax. = 359 °C) and MCNC (Tonset = 181 °C and Tmax = 359 °C) bioplastics was observed when the thermogravimetric results were evaluated (Figure 9). In other words, the presence of nanocrystals did not affect the thermal resistance of the film.

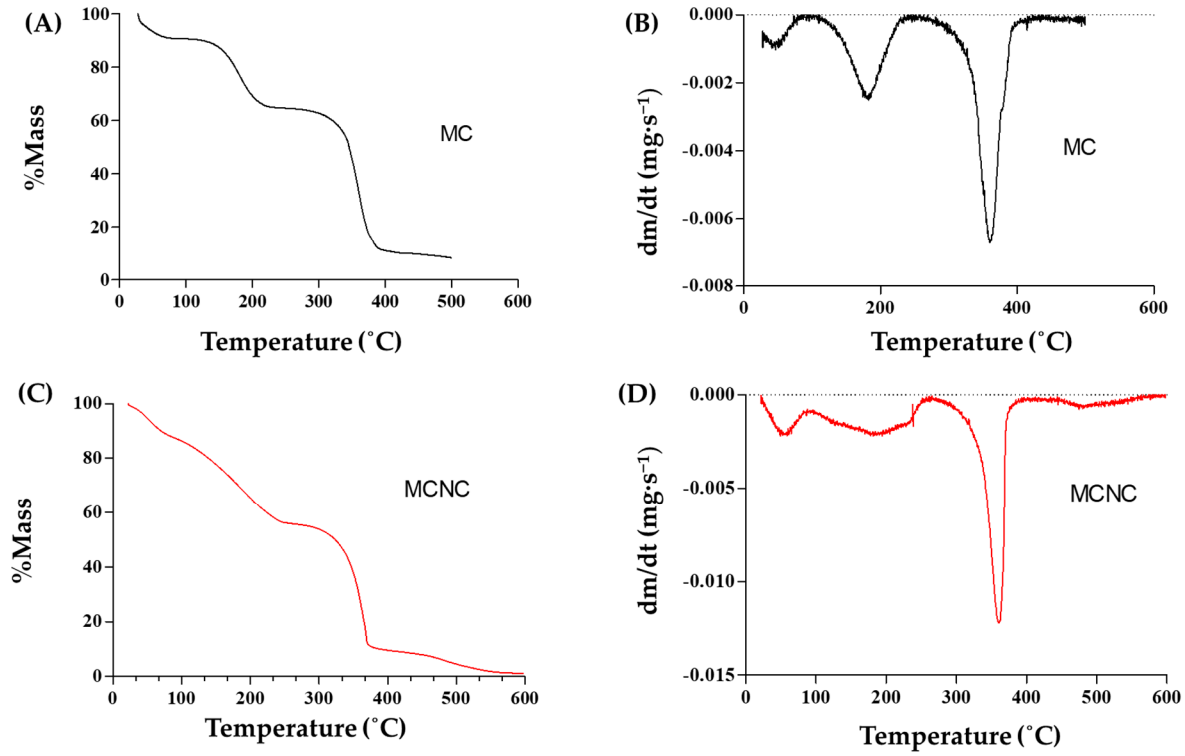

Figure 9. Thermogravimetry of bioplastics. (**A**,**B**) TGA curve and 1° curve derived from MC bioplastic with 0.0% CNC. (**C**,**D**) TGA curve and 1° curve derived from the MCNC bioplastic with 0.6% CNC.

Based on the profile of mass loss between 100 °C and 200 °C, MCNC films presented less moisture than the MC films, which agrees with the results presented for moisture content. This behavior can be explained by the capacity of CNCs to establish bonds with the MC polymeric matrix, thus preventing water molecule absorption. Other studies with CNC have also demonstrated that the thermal resistance of the studied bioplastics did not increase with the addition of cellulose nanocrystals extracted by acid hydrolysis with sulfuric acid [66,67].

3.7.3. Tensile Test

The variables studied in the mechanical resistance test were tensile strength (TS), Young's modulus (YM), and percentage elongation at break (%EB) (Table 4). The addition of cellulose nanocrystals to the methylcellulose film resulted in a 37.11-fold increase in %EB (1.56% for the MC film and 57.90% for the MCNC 0.6% film) and a 280-fold decrease in YM (0.42 GPa for the MC film and 0.0015 GPa for the MCNC 0.6% film) ($p < 0.05$). Clearly, the addition of cellulose nanocrystals significantly increased the flexibility and ductility of MC films.

Table 4. Film mechanical tests results.

Tests	MC	MCNC 0.6%
Tensile strength (MPa)	25 ^{a} * ± 4	22 ^{a} ± 7
Young's modulus (GPa)	0.42 ^{a} ± 0.01	0.0015 ^{b} ± 0.0007
% Elongation at break	1.6 ^{a} ± 0.1	58 ^{b} ± 11

* $^{a–b}$: In the same row, means followed by same superscript letters have no statistical difference between each other ($p > 0.05$).

The increase in elongation and the reduction in tensile strength are not commonly reported effects in the literature regarding the incorporation of cellulose nanocrystals into polymer matrices, whether synthetic or biopolymeric. However, some stud-

ies have described similar behavior in different composites, such as in the study by Cherpinski et al. (2018) [68], where the addition of nanofibrillated cellulose and lignocellulosic nanofibrils to a polyhydroxyalkanoate (PHA) matrix resulted in an increase in elongation percentage and a decrease in tensile strength when compared to pure PHA. The tensile strength of pure PHB (poly(3-hydroxybutyrate)) increased from 14.5 MPa to 22.5 MPa, while elongation at break increased from 2.8% to 6.6% in formulations containing nanofibrillated cellulose (PHB/CNF/PHB). Similar results were observed by Nascimento et al. (2021) [69], who reported that incorporating cellulose nanocrystals into an epoxy matrix caused a slight decrease in tensile strength accompanied by a significant increase in elongation. The tensile strength decreased from 73 MPa (pure epoxy) to 67.6 MPa with 7% nanocrystals, whereas the flexural modulus increased from 1.60 GPa to 2.10 GPa.

Likewise, Jo et al. (2021) [70] demonstrated that the addition of cellulose nanocrystals modified with organosiloxanes to a PHA matrix led to a 301% increase in elongation, along with a slight reduction in Young's modulus. Although cellulose nanocrystals are widely recognized for their highly rigid nature and therefore typically act as reinforcing agents, various structural and surface-related factors can cause these nanomaterials to produce the opposite effect: increased elongation and reduced Young's modulus in polymer matrices. This atypical behavior can be explained by three interconnected mechanisms.

First, at low concentrations and when well dispersed, CNCs can behave similarly to a plasticizer. In this condition, their surfaces interact with the polymer chains, partially reducing intermolecular interactions within the matrix, increasing segmental mobility, and creating zones of greater flexibility. Moreover, CNCs can alter the crystallization kinetics and degree of crystallinity of the matrix, leading to the formation of less perfect or less dense crystals, which favors greater deformability of the material. Some authors, such as Zhang et al. (2019) [71] and Leite et al. (2020) [72], obtained similar results and conclusions when adding cellulose nanocrystals to polyhydroxybutyrate and gelatin polymer matrices, respectively.

Second, when CNCs contain residual lignin, the flexibility of the composite tends to increase even further. Lignin, being an amorphous, hydrophobic, and structurally irregular aromatic polymer, disrupts the rigidity normally associated with highly purified CNCs by reducing the density of hydrogen bonding within both CNC–CNC and CNC–matrix interactions. These less-rigid interfacial regions act as stress-dissipating zones, allowing greater elongation before break.

Finally, the presence of inorganic impurities—particularly sodium sulfate (Na_2SO_4) remaining from the sulfuric acid hydrolysis process—also contributes to this more ductile mechanical behavior. Adsorbed sulfate ions can compete with hydroxyl groups for electrostatic interactions, partially blocking bonding sites and reducing the stiffness of hydrogen-bonding networks. These impurities also influence the crystalline organization of CNCs, decreasing their intrinsic rigidity, and can modify their surface charge, affecting dispersion and creating more flexible microdomains within the matrix.

Thus, the combination of these three factors—plasticizer-like behavior of well-dispersed CNCs, flexibilization caused by residual lignin, and the reduction in intermolecular interactions due to impurities such as Na_2SO_4—clearly explains why, under certain conditions, the incorporation of CNCs can simultaneously lead to higher elongation and lower Young's modulus in polymer films.

In addition to this factor, there is also the wide distribution of nanocrystal dimensions (Figure 2D). The diversity in the dimensions of cellulose nanocrystals allows for an increase in the number of intermolecular bonds with different distances. Consequently, the polymer matrix can adjust its mobility according to the change in applied axial force. The low crystallinity also decreases the likelihood of film stiffening and, consequently, reduces

Young's modulus, as the less organized structure of the crystals allows for a greater number of atomic movements [73,74].

The reinforcing efficiency of cellulose nanocrystals (CNCs) in composites strongly depends on the homogeneous dispersion and uniformity of the particles within the polymer matrix [4]. When CNCs are not uniformly distributed, some regions of the matrix are poorly reinforced while others may contain aggregates, creating structural discontinuities and local stress concentrations that lead to premature failure and reductions in tensile strength and modulus [75]. Furthermore, the presence of a bimodal or multimodal particle size distribution contributes to a heterogeneous microstructure: larger particles tend to form aggregates, while smaller particles may not efficiently fill the volume, resulting in alternating regions of reinforced and weak areas. The combination of these factors—non-uniformity, aggregation, and bimodal distribution—significantly compromises the mechanical properties of the composite, which may exhibit unusual behavior in mechanical testing.

The inclusion of cellulose nanocrystals in the methylcellulose film did not yield a significant ($p > 0.05$) impact on the tensile strength (TS) of the film. The tensile strength of the methylcellulose (MC) film measured 24.64 MPa, while for the 0.6% methylcellulose nanocrystals (MCNCs) film, it stood at 21.71 MPa. In the context of integrating cellulose nanocrystals into a compatible polymer matrix, the primary factor influencing tensile strength revolves around the crystallinity of the cellulose nanocrystals and/or their agglomeration.

The nanocrystals generated in this investigation exhibit a moderate crystallinity index and are not meticulously arranged to the extent of hindering the movement of the methylcellulose polymer matrix. Consequently, they neither elevate nor diminish the tensile strength of the matrix. Moreover, the cellulose nanocrystals demonstrate uniform dispersion within the film, mitigating the impact of potential heterogeneous nucleation that could alter the polymer crystallization process and impact its stiffness. This hypothesis finds support in studies such as those of Zhang et al. (2022) [76] and Wang et al. (2019) [74], which showcase an uptick in tensile strength corresponding to higher cellulose nanocrystal concentrations and/or increased crystallinity of these nanocrystals.

4. Conclusions

The results presented in this work demonstrate that CNCs extracted from low-quality coffee beans exhibit physicochemical characteristics with potential for biotechnological applications, particularly due to their crystallinity index and thermal resistance. The incorporation of cellulose nanocrystals into the methylcellulose matrix significantly increased the elongation capacity while reducing the stiffness of the films, resulting in materials that are notably more flexible and less rigid. At a concentration of 0.6% CNC, the MCNC films showed the most pronounced improvement in mechanical behavior, confirming the ability of the nanoparticles to soften the matrix and enhance its deformability. In addition to this mechanical flexibilization, CNC incorporation reduced the moisture content of the films, maintained their high transparency, and improved their UV light barrier property.

These combined characteristics are highly desirable for the development of bio-based food packaging materials. Furthermore, the use of agricultural residues—such as discarded coffee beans—as a source of CNCs represents an environmentally beneficial approach that adds value to materials that would otherwise be discarded and contributes to sustainable development.

Supplementary Materials: The following supporting information can be downloaded at: https://www.mdpi.com/article/10.3390/resources14120191/s1, Supplementary Material S1: Glucose concentration measure and Supplementary Material S2: CNC stability test.

Author Contributions: Conceptualization, G.d.S.P. and T.A.d.O.M.; methodology, G.d.S.P.; formal analysis, G.d.S.P. and J.S.P.; investigation, G.d.S.P., J.S.P., A.P.A., K.V.R.V. and L.F.A.; resources, T.A.d.O.M.; writing—original draft preparation, G.d.S.P.; writing—review and editing, C.S.M., T.V.d.O., D.d.J.S., T.A.d.O.M., V.G.L.S., S.O.F., E.T.C.M. and A.d.O.B.R.; visualization, T.V.d.O., D.d.J.S., T.A.d.O.M., V.G.L.S., E.T.C.M., S.O.F. and A.d.O.B.R.; supervision, T.A.d.O.M.; project administration, T.A.d.O.M.; funding acquisition, E.T.C.M. and T.A.d.O.M. All authors have read and agreed to the published version of the manuscript.

Funding: This research was funded by Coordernação de Aperfeiçoamento de Pessoal de Nível Superior (CAPES); Consórcio Pesquisa Café; Conselho Nacional de Desenvolvimento Científico e Tecnológico (CNPq); and Fundação de Amparo à Pesquisa do Estado de Minas Gerais (FAPEMIG). V.G.L.S also acknowledges the Foundation for Science and Technology (FCT) from the Ministry of Education, Science and Innovation (MECI) for funding the individual contract (https://doi.org/10.54499/2023.09446.CEECIND/CP2836/CT0011).

Data Availability Statement: All data are available in the manuscript or Supplement Materials.

Acknowledgments: We are grateful to the research laboratories at the Federal University of Viçosa (UFV), which kindly assisted in the development of the analyses in this work, especially the Food Packaging Laboratory/UFV and the Nanoscopy Center/UFV.

Conflicts of Interest: Author Eveline Teixeira Caixeta Moura was employed by the company Embrapa Café. The remaining authors declare that the research was conducted in the absence of any commercial or financial relationships that could be construed as a potential conflict of interest.

References

1. Przygrodzka, K.; Chareza, M.; Banaszek, A.; Zielińska, B.; Ekiert, E.; Drozd, R. Bacterial Cellulose Production by Komagateibacter Xylinus with the Use of Enzyme-Degraded Oligo- and Polysaccharides as the Substrates. *Appl. Sci.* **2022**, *12*, 12673. [CrossRef]
2. Etale, A.; Onyianta, A.J.; Turner, S.R.; Eichhorn, S.J. Cellulose: A Review of Water Interactions, Applications in Composites, and Water Treatment. *Chem. Rev.* **2023**, *123*, 2016–2048. [CrossRef] [PubMed]
3. Emenike, E.C.; Iwuozor, K.O.; Saliu, O.D.; Ramontja, J.; Adeniyi, A.G. Advances in the Extraction, Classification, Modification, Emerging and Advanced Applications of Crystalline Cellulose: A Review. *Carbohydr. Polym. Technol. Appl.* **2023**, *6*, 100337. [CrossRef]
4. Pires, J.R.A.; Souza, V.G.L.; Fernando, A.L. Valorization of Energy Crops as a Source for Nanocellulose Production—Current Knowledge and Future Prospects. *Ind. Crops Prod.* **2019**, *140*, 111642. [CrossRef]
5. Souza, A.L.; Souza, V.G.L.; Jesus, M.; Mata, F.; Oliveira, T.V.d.; Soares, N.d.F.F. Modification of Cellulose Nanocrystals Using Polydopamine for the Modulation of Biodegradable Packaging, Polymeric Films: A Mini Review. *Sustainability* **2025**, *17*, 5633. [CrossRef]
6. Anusiya, G.; Jaiganesh, R. A Review on Fabrication Methods of Nanofibers and a Special Focus on Application of Cellulose Nanofibers. *Carbohydr. Polym. Technol. Appl.* **2022**, *4*, 100262. [CrossRef]
7. Yi, T.; Zhao, H.; Mo, Q.; Pan, D.; Liu, Y.; Huang, L.; Xu, H.; Hu, B.; Song, H. From Cellulose to Cellulose Nanofibrils—A Comprehensive Review of the Preparation and Modification of Cellulose Nanofibrils. *Materials* **2020**, *13*, 5062. [CrossRef]
8. Ullah, M.W.; Alabbosh, K.F.; Fatima, A.; Islam, S.U.; Manan, S.; Ul-Islam, M.; Yang, G. Advanced Biotechnological Applications of Bacterial Nanocellulose-Based Biopolymer Nanohybrids: A Review. *Adv. Ind. Eng. Polym. Res.* **2024**, *7*, 100–121. [CrossRef]
9. Razali, S.A.; Azwadi, N.; Sidik, C.; Koten, H. Cellulose Nanocrystals: A Brief Review on Properties and General Applications. *J. Adv. Res. Des.* **2019**, *60*, 1–15.
10. Omran, A.A.B.; Mohammed, A.A.B.A.; Sapuan, S.M.; Ilyas, R.A.; Asyraf, M.R.M.; Rahimian Koloor, S.S.; Petrů, M. Micro- and Nanocellulose in Polymer Composite Materials: A Review. *Polymers* **2021**, *13*, 231. [CrossRef]
11. Mohammadpour-Haratbar, A.; Boraei, S.B.A.; Munir, M.T.; Zare, Y.; Rhee, K.Y. A Model for Tensile Strength of Cellulose Nanocrystals Polymer Nanocomposites. *Ind. Crops Prod.* **2024**, *213*, 118458. [CrossRef]
12. Chen, W.; Yu, H.; Lee, S.-Y.; Wei, T.; Li, J.; Fan, Z. Nanocellulose: A Promising Nanomaterial for Advanced Electrochemical Energy Storage. *Chem. Soc. Rev.* **2018**, *47*, 2837–2872. [CrossRef]
13. Kádár, R.; Spirk, S.; Nypelö, T. Cellulose Nanocrystal Liquid Crystal Phases: Progress and Challenges in Characterization Using Rheology Coupled to Optics, Scattering, and Spectroscopy. *ACS Nano* **2021**, *15*, 7931–7945. [CrossRef]
14. Gomri, C.; Cretin, M.; Semsarilar, M. Recent Progress on Chemical Modification of Cellulose Nanocrystal (CNC) and Its Application in Nanocomposite Films and Membranes-A Comprehensive Review. *Carbohydr. Polym.* **2022**, *294*, 119790. [CrossRef]

15. Perdoch, W.; Cao, Z.; Florczak, P.; Markiewicz, R.; Jarek, M.; Olejnik, K.; Mazela, B. Influence of Nanocellulose Structure on Paper Reinforcement. *Molecules* **2022**, *27*, 4696. [CrossRef]
16. Aziz, T.; Farid, A.; Haq, F.; Kiran, M.; Ullah, A.; Zhang, K.; Li, C.; Ghazanfar, S.; Sun, H.; Ullah, R.; et al. A Review on the Modification of Cellulose and Its Applications. *Polymers* **2022**, *14*, 3206. [CrossRef]
17. Embrapa Safra Dos Cafés Do Brasil de Coffea Arábica Atinge 38.90 Milho~es de Sacas e Equivale a 40% Da Produção Mundial Dessa Espécie. Available online: https://www.embrapa.br/en/busca-de-noticias/-/noticia/86470599/artigo--safra-dos-cafes-do-brasil-de-coffea-arabica-atinge-3890-milhoes-de-sacas-e-equivale-a-40-da-producao-mundial-dessa-especie#: :text=tantodeC.,arabicacomodeC.,colhidonoplanetae (accessed on 10 August 2024).
18. Conab Companhia Nacional de Abastecimento Produção de Café Cresce 8.2% Em 2023 e Chega a 55.1 Milhões de Sacas. Available online: https://www.conab.gov.br/ultimas-noticias/5175-producao-de-cafe-esta-estimada-em-54-36-milhoes-de-sacas-3-maior-na-serie-historica (accessed on 20 September 2024).
19. Embrapa Produtividade Média Dos Cafés Do Brasil Equivale a 28.9 Sacas Por Hectare Em 2023. Available online: https://www.embrapa.br/busca-de-noticias/-/noticia/80992551/produtividade-media-dos-cafes-do-brasil-equivale-a-289-sacas-por-hectare-em-2023/ (accessed on 10 July 2024).
20. Dey, D.; Gyeltshen, T.; Aich, A.; Naskar, M.; Roy, A. Climate Adaptive Crop-Residue Management for Soil-Function Improvement; Recommendations from Field Interventions at Two Agro-Ecological Zones in South Asia. *Environ. Res.* **2020**, *183*, 109164. [CrossRef]
21. Raza, M.H.; Abid, M.; Faisal, M.; Yan, T.; Akhtar, S.; Adnan, K.M.M. Environmental and Health Impacts of Crop Residue Burning: Scope of Sustainable Crop Residue Management Practices. *Int. J. Environ. Res. Public Health* **2022**, *19*, 4753. [CrossRef] [PubMed]
22. Gondim, F.F.; Rodrigues, J.G.P.; Aguiar, V.O.; de Fátima Vieira Marques, M.; Monteiro, S.N. Biocomposites of Cellulose Isolated from Coffee Processing By-Products and Incorporation in Poly(Butylene Adipate-Co-Terephthalate) (PBAT) Matrix: An Overview. *Polymers* **2024**, *16*, 314. [CrossRef] [PubMed]
23. Kanai, N.; Honda, T.; Yoshihara, N.; Oyama, T.; Naito, A.; Ueda, K.; Kawamura, I. Structural Characterization of Cellulose Nanofibers Isolated from Spent Coffee Grounds and Their Composite Films with Poly(Vinyl Alcohol): A New Non-Wood Source. *Cellulose* **2020**, *27*, 5017–5028. [CrossRef]
24. Bondam, A.F.; Diolinda da Silveira, D.; Pozzada dos Santos, J.; Hoffmann, J.F. Phenolic Compounds from Coffee By-Products: Extraction and Application in the Food and Pharmaceutical Industries. *Trends Food Sci. Technol.* **2022**, *123*, 172–186. [CrossRef]
25. Silva, M.d.O.; Honfoga, J.N.B.; Medeiros, L.L.d.; Madruga, M.S.; Bezerra, T.K.A. Obtaining Bioactive Compounds from the Coffee Husk (*Coffea arabica* L.) Using Different Extraction Methods. *Molecules* **2020**, *26*, 46. [CrossRef]
26. Morais, J.P.S.; Rosa, M.d.F.; Marconcini, J.M. *Procedimentos Para Análise Lignocelulósica—Documento 236*; Embrapa: Campina Grande, Brazil, 2010; ISBN 0103-0205.
27. Martim, J.D. XPowderX, (Version 2023.04.24) [Software]. 2023. Available online: https://www.xpowder.com (accessed on 10 June 2025).
28. Mclellan, M.R.; Lind, L.R.; Kime, R.W. Hue Angle Determinations and Statistical Analysis for Multiquadrant Hunter L,a,b Data. *J. Food Qual.* **1995**, *18*, 235–240. [CrossRef]
29. Zhao, J.; Wang, Y.; Liu, C. Film Transparency and Opacity Measurements. *Food Anal. Methods* **2022**, *15*, 2840–2846. [CrossRef]
30. Standard, A. ASTM Standard Test Method for Tensile Properties of Thin Plastic Sheeting. *Am. Soc. Test. Mater. West* **2012**, *D882-12*, 1–11. [CrossRef]
31. Ho, M.C.; Ong, V.Z.; Wu, T.Y. Potential Use of Alkaline Hydrogen Peroxide in Lignocellulosic Biomass Pretreatment and Valorization—A Review. *Renew. Sustain. Energy Rev.* **2019**, *112*, 75–86. [CrossRef]
32. Martins, R.P.; Schmatz, A.A.; de Freita, L.A.; Mutton, M.J.R.; Brienzo, M. Solubilization of Hemicellulose and Fermentable Sugars from Bagasse, Stalks, and Leaves of Sweet Sorghum. *Ind. Crops Prod.* **2021**, *170*, 113813. [CrossRef]
33. Widjaja, T.; Nurkhamidah, S.; Altway, A.; Rohmah, A.A.Z.; Saepulah, F. Chemical Pre-Treatments Effect for Reducing Lignin on Cocoa Pulp Waste for Biogas Production. In Proceedings of the 4th International Seminar on Chemistry, Surabaya, Indonesia, 7–8 October 2020; Volume 020058, p. 020058.
34. Benali, M.; Oulmekki, A.; Toyir, J. The Impact of the Alkali-Bleaching Treatment on the Isolation of Natural Cellulosic Fibers from Juncus Effesus L Plant. *Fibers Polym.* **2024**, *25*, 525–533. [CrossRef]
35. Ding, J.; Liang, L.; Meng, X.; Yang, F.; Pu, Y.; Ragauskas, A.J.; Yoo, C.G.; Yu, C. The Physiochemical Alteration of Flax Fibers Structuring Components after Different Scouring and Bleaching Treatments. *Ind. Crops Prod.* **2021**, *160*, 113112. [CrossRef]
36. Melesse, G.T.; Hone, F.G.; Mekonnen, M.A. Extraction of Cellulose from Sugarcane Bagasse Optimization and Characterization. *Adv. Mater. Sci. Eng.* **2022**, *2022*, 1712207. [CrossRef]
37. Rasheed, H.A.; Adeleke, A.A.; Nzerem, P.; Olosho, A.I.; Ogedengbe, T.S.; Jesuloluwa, S. Isolation, Characterization and Response Surface Method Optimization of Cellulose from Hybridized Agricultural Wastes. *Sci. Rep.* **2024**, *14*, 14310. [CrossRef] [PubMed]
38. Mancera, A.; Fierro, V.; Pizzi, A.; Dumarçay, S.; Gérardin, P.; Velásquez, J.; Quintana, G.; Celzard, A. Physicochemical Characterisation of Sugar Cane Bagasse Lignin Oxidized by Hydrogen Peroxide. *Polym. Degrad. Stab.* **2010**, *95*, 470–476. [CrossRef]

39. Khenblouche, A.; Bechki, D.; Gouamid, M.; Charradi, K.; Segni, L.; Hadjadj, M.; Boughali, S. Extraction and Characterization of Cellulose Microfibers from Retama Raetam Stems. *Polímeros* **2019**, *29*, e2019011. [CrossRef]
40. Doh, H.; Lee, M.H.; Whiteside, W.S. Physicochemical Characteristics of Cellulose Nanocrystals Isolated from Seaweed Biomass. *Food Hydrocoll.* **2020**, *102*, 105542. [CrossRef]
41. Matebie, B.Y.; Tizazu, B.Z.; Kadhem, A.A.; Venkatesa Prabhu, S. Synthesis of Cellulose Nanocrystals (CNCs) from Brewer's Spent Grain Using Acid Hydrolysis: Characterization and Optimization. *J. Nanomater.* **2021**, *2021*, 7133154. [CrossRef]
42. Rasheed, M.; Jawaid, M.; Parveez, B.; Zuriyati, A.; Khan, A. Morphological, Chemical and Thermal Analysis of Cellulose Nanocrystals Extracted from Bamboo Fibre. *Int. J. Biol. Macromol.* **2020**, *160*, 183–191. [CrossRef] [PubMed]
43. Deb Dutta, S.; Patel, D.K.; Ganguly, K.; Lim, K.-T. Isolation and Characterization of Cellulose Nanocrystals from Coffee Grounds for Tissue Engineering. *Mater. Lett.* **2021**, *287*, 129311. [CrossRef]
44. Akinjokun, A.I.; Petrik, L.F.; Ogunfowokan, A.O.; Ajao, J.; Ojumu, T.V. Isolation and Characterization of Nanocrystalline Cellulose from Cocoa Pod Husk (CPH) Biomass Wastes. *Heliyon* **2021**, *7*, e06680. [CrossRef] [PubMed]
45. Panchal, P.; Ogunsona, E.; Mekonnen, T. Trends in Advanced Functional Material Applications of Nanocellulose. *Processes* **2018**, *7*, 10. [CrossRef]
46. Babaei-Ghazvini, A.; Acharya, B. Influence of Cellulose Nanocrystal Aspect Ratio on Shear Force Aligned Films: Physical and Mechanical Properties. *Carbohydr. Polym. Technol. Appl.* **2022**, *3*, 100217. [CrossRef]
47. Wu, Q.; Li, X.; Li, Q.; Wang, S.; Luo, Y. Estimation of Aspect Ratio of Cellulose Nanocrystals by Viscosity Measurement: Influence of Aspect Ratio Distribution and Ionic Strength. *Polymers* **2019**, *11*, 781. [CrossRef]
48. Kassab, Z.; Kassem, I.; Hannache, H.; Bouhfid, R.; Qaiss, A.E.K.; El Achaby, M. Tomato Plant Residue as New Renewable Source for Cellulose Production: Extraction of Cellulose Nanocrystals with Different Surface Functionalities. *Cellulose* **2020**, *27*, 4287–4303. [CrossRef]
49. Gabriel, T.; Belete, A.; Hause, G.; Neubert, R.H.H.; Gebre-Mariam, T. Isolation and Characterization of Cellulose Nanocrystals from Different Lignocellulosic Residues: A Comparative Study. *J. Polym. Environ.* **2021**, *29*, 2964–2977. [CrossRef]
50. Holder, C.F.; Schaak, R.E. Tutorial on Powder X-Ray Diffraction for Characterizing Nanoscale Materials. *ACS Nano* **2019**, *13*, 7359–7365. [CrossRef]
51. Huntley, C.J.; Crews, K.D.; Abdalla, M.A.; Russell, A.E.; Curry, M.L. Influence of Strong Acid Hydrolysis Processing on the Thermal Stability and Crystallinity of Cellulose Isolated from Wheat Straw. *Int. J. Chem. Eng.* **2015**, *2015*, 658163. [CrossRef]
52. Fitriani, F.; Aprilia, S.; Arahman, N.; Bilad, M.R.; Amin, A.; Huda, N.; Roslan, J. Isolation and Characterization of Nanocrystalline Cellulose Isolated from Pineapple Crown Leaf Fiber Agricultural Wastes Using Acid Hydrolysis. *Polymers* **2021**, *13*, 4188. [CrossRef]
53. Fawcett, T.G.; Crowder, C.E.; Kabekkodu, S.N.; Needham, F.; Kaduk, J.A.; Blanton, T.N.; Petkov, V.; Bucher, E.; Shpanchenko, R. Reference Materials for the Study of Polymorphism and Crystallinity in Cellulosics. *Powder Diffr.* **2013**, *28*, 18–31. [CrossRef]
54. Gražulis, S.; Chateigner, D.; Downs, R.T.; Yokochi, A.F.T.; Quirós, M.; Lutterotti, L.; Manakova, E.; Butkus, J.; Moeck, P.; Le Bail, A. Crystallography Open Database—An Open-Access Collection of Crystal Structures. *J. Appl. Crystallogr.* **2009**, *42*, 726–729. [CrossRef]
55. Farooq Adil, S.; Bhat, V.S.; Batoo, K.M.; Imran, A.; Assal, M.E.; Madhusudhan, B.; Khan, M.; Al-Warthan, A. Isolation and Characterization of Nanocrystalline Cellulose from Flaxseed Hull: A Future Onco-Drug Delivery Agent. *J. Saudi Chem. Soc.* **2020**, *24*, 374–379. [CrossRef]
56. Frost, A.B.; Johan Foster, E. Isolation of Thermally Stable Cellulose Nanocrystals from Spent Coffee Grounds via Phosphoric Acid Hydrolysis. *J. Renew. Mater.* **2020**, *8*, 187–203. [CrossRef]
57. López-Beceiro, J.; Díaz-Díaz, A.M.; Álvarez-García, A.; Tarrío-Saavedra, J.; Naya, S.; Artiaga, R. The Complexity of Lignin Thermal Degradation in the Isothermal Context. *Processes* **2021**, *9*, 1154. [CrossRef]
58. Sabaruddin, F.A.; Paridah, M.T. Effect of Lignin on the Thermal Properties of Nanocrystalline Prepared from Kenaf Core. *IOP Conf. Ser. Mater. Sci. Eng.* **2018**, *368*, 012039. [CrossRef]
59. Kumar, A.; Singh Negi, Y.; Choudhary, V.; Kant Bhardwaj, N. Characterization of Cellulose Nanocrystals Produced by Acid-Hydrolysis from Sugarcane Bagasse as Agro-Waste. *J. Mater. Phys. Chem.* **2020**, *2*, 1–8. [CrossRef]
60. Pereira, P.H.F.; Ornaghi Júnior, H.L.; Coutinho, L.V.; Duchemin, B.; Cioffi, M.O.H. Obtaining Cellulose Nanocrystals from Pineapple Crown Fibers by Free-Chlorite Hydrolysis with Sulfuric Acid: Physical, Chemical and Structural Characterization. *Cellulose* **2020**, *27*, 5745–5756. [CrossRef]
61. Zhu, P.; Feng, L.; Ding, Z.; Bai, X. Preparation of Spherical Cellulose Nanocrystals from Microcrystalline Cellulose by Mixed Acid Hydrolysis with Different Pretreatment Routes. *Int. J. Mol. Sci.* **2022**, *23*, 10764. [CrossRef]
62. Leppänen, I.; Hokkanen, A.; Österberg, M.; Vähä-Nissi, M.; Harlin, A.; Orelma, H. Hybrid Films from Cellulose Nanomaterials—Properties and Defined Optical Patterns. *Cellulose* **2022**, *29*, 8551–8567. [CrossRef]

63. Zhang, Y.; Haque, A.N.M.A.; Naebe, M. Lignin–Cellulose Nanocrystals from Hemp Hurd as Light-Coloured Ultraviolet (UV) Functional Filler for Enhanced Performance of Polyvinyl Alcohol Nanocomposite Films. *Nanomaterials* **2021**, *11*, 3425. [CrossRef] [PubMed]
64. Lin, M.; Yang, L.; Zhang, H.; Xia, Y.; He, Y.; Lan, W.; Ren, J.; Yue, F.; Lu, F. Revealing the Structure-Activity Relationship between Lignin and Anti-UV Radiation. *Ind. Crops Prod.* **2021**, *174*, 114212. [CrossRef]
65. Kim, H.-J.; Kwon, H.-J.; Jeon, S.; Park, J.-W.; Sunthornvarabhas, J.; Sriroth, K. Electrical and Optical Properties of Nanocellulose Films and Its Nanocomposites. In *Handbook of Polymer Nanocomposites. Processing, Performance and Application*; Springer: Berlin/Heidelberg, Germany, 2015; pp. 395–432.
66. Agustin, M.B.; Ahmmad, B.; Alonzo, S.M.M.; Patriana, F.M. Bioplastic Based on Starch and Cellulose Nanocrystals from Rice Straw. *J. Reinf. Plast. Compos.* **2014**, *33*, 2205–2213. [CrossRef]
67. Blilid, S.; Kędzierska, M.; Miłowska, K.; Wrońska, N.; El Achaby, M.; Katir, N.; Belamie, E.; Alonso, B.; Lisowska, K.; Lahcini, M.; et al. Phosphorylated Micro- and Nanocellulose-Filled Chitosan Nanocomposites as Fully Sustainable, Biologically Active Bioplastics. *ACS Sustain. Chem. Eng.* **2020**, *8*, 18354–18365. [CrossRef]
68. Cherpinski, A.; Torres-giner, S.; Vartiainen, J.; Peresin, M.; Lahtinen, P.; Lagaron, J.M. Improving the Water Resistance of Nanocellulose-Based Films with Polyhydroxyalkanoates Processed by the Electrospinning Coating Technique. *Cellulose* **2018**, *25*, 1291–1307. [CrossRef]
69. Nascimento, N.R.; Pinheiro, I.F.; Alves, G.F.; Mei, L.H.I.; Neto, J.C.M.; Morales, A.R. Role of Cellulose Nanocrystals in Epoxy-Based Nanocomposites: Mechanical Properties, Morphology and Thermal Behavior. *Polímeros Ciência e Tecnol.* **2021**, *31*, e2021034. [CrossRef]
70. Jo, J.; Kim, H.; Jeong, S.; Park, C.; Hwang, H.S.; Koo, B. Changes in Mechanical Properties of Polyhydroxyalkanoate with Double Silanized Cellulose Nanocrystals Using Different Organosiloxanes. *Nanomaterials* **2021**, *11*, 1542. [CrossRef]
71. Zhang, B.; Huang, C.; Zhao, H.; Wang, J.; Yin, C.; Zhang, L.; Zhao, Y. Effects of Cellulose Nanocrystals and Cellulose Nanofibers on the Structure and Properties of Polyhydroxybutyrate Nanocomposites. *Polymers* **2019**, *11*, 2063. [CrossRef]
72. Leite, L.S.F.; Bilatto, S.; Paschoalin, R.T.; Soares, A.C.; Moreira, F.K.V.; Oliveira, O.N.; Mattoso, L.H.C.; Bras, J. Eco-Friendly Gelatin Films with Rosin-Grafted Cellulose Nanocrystals for Antimicrobial Packaging. *Int. J. Biol. Macromol.* **2020**, *165*, 2974–2983. [CrossRef] [PubMed]
73. Coelho, C.C.d.S.; Silva, R.B.S.; Carvalho, C.W.P.; Rossi, A.L.; Teixeira, J.A.; Freitas-Silva, O.; Cabral, L.M.C. Cellulose Nanocrystals from Grape Pomace and Their Use for the Development of Starch-Based Nanocomposite Films. *Int. J. Biol. Macromol.* **2020**, *159*, 1048–1061. [CrossRef]
74. Wang, Z.; Yao, Z.; Zhou, J.; He, M.; Jiang, Q.; Li, A.; Li, S.; Liu, M.; Luo, S.; Zhang, D. Improvement of Polylactic Acid Film Properties through the Addition of Cellulose Nanocrystals Isolated from Waste Cotton Cloth. *Int. J. Biol. Macromol.* **2019**, *129*, 878–886. [CrossRef] [PubMed]
75. Pires, J.R.A.; Souza, V.G.L.; Gomes, L.A.; Coelhoso, I.M.; Godinho, M.H.; Fernando, A.L. Micro and Nanocellulose Extracted from Energy Crops as Reinforcement Agents in Chitosan Films. *Ind. Crops Prod.* **2022**, *186*, 115247. [CrossRef]
76. Zhang, Y.; Wang, X.; Li, Y.; Li, J. Cellulose Nanocrystals Composites with Excellent Thermal Stability and High Tensile Strength for Preparing Flexible Resistance Strain Sensors. *Carbohydr. Polym. Technol. Appl.* **2022**, *3*, 100214. [CrossRef]

Disclaimer/Publisher's Note: The statements, opinions and data contained in all publications are solely those of the individual author(s) and contributor(s) and not of MDPI and/or the editor(s). MDPI and/or the editor(s) disclaim responsibility for any injury to people or property resulting from any ideas, methods, instructions or products referred to in the content.